Summer Antarctic sea ice as seen by ASAR and AMSR-E and observed during two IPY field cruises: a case study

Ahmet E. TEKELI,[1] Stefan KERN,[2] Stephen F. ACKLEY,[1]
Burcu OZSOY-CICEK,[1] Hongjie XIE[1]

[1]Department of Geological Sciences, University of Texas at San Antonio, 1 UTSA Circle, San Antonio, TX 78249, USA
E-mail: ahmet.tekeli@utsa.edu
[2]Center for Marine and Atmospheric Science, CliSAP/KlimaCampus, University of Hamburg, Grindelberg 5,
D-20144 Hamburg, Germany

ABSTRACT. Envisat Advanced Synthetic Aperture Radar (ASAR) Wide Swath Mode (WSM) images are used to derive C-band HH-polarization normalized radar cross sections (NRCS). These are compared with ice-core analysis and visual ship-based observations of snow and ice properties observed according to the Antarctic Sea Ice Processes and Climate (ASPeCt) protocol during two International Polar Year summer cruises (*Oden* 2008 and *Palmer* 2009) in West Antarctica. Thick first-year (TFY) and multi-year (MY) ice were the dominant ice types. The NRCS value ranges between -16.3 ± 1.1 and $-7.6 \pm 1.0\,dB$ for TFY ice, and is $-12.6 \pm 1.3\,dB$ for MY ice; for TFY ice, NRCS values increase from $\sim -15\,dB$ to $-9\,dB$ from December/January to mid-February. In situ and ASPeCt observations are not, however, detailed enough to interpret the observed NRCS change over time. Co-located Advanced Microwave Scanning Radiometer–Earth Observing System (AMSR-E) vertically polarized 37 GHz brightness temperatures (TB37V), 7 day and 1 day averages as well as the TB37V difference between ascending and descending AMSR-E overpasses suggest the low NRCS values (–15 dB) are associated with snowmelt being still in progress, while the change towards higher NRCS values (–9 dB) is caused by commencement of melt–refreeze cycles after about mid-January.

INTRODUCTION

Sea ice is a sensitive indicator of climate change (Lubin and Massom, 2006). With its high albedo relative to the ocean and low thermal conductivity, it regulates the ocean–atmosphere heat, moisture, and energy exchange (Smith and others, 1990; Meier and Stroeve, 2008). Variations in sea-ice albedo and these exchanges are difficult to monitor on a basin-wide scale. Satellite data can support the determination of the sea-ice albedo and the mentioned fluxes by providing detailed ice-property distribution information by, for example, classification of different ice types, mapping of the sea-ice roughness distribution, or identification of leads and polynyas (Jeffries, 1998; Lubin and Massom, 2006).

Detailed ice information at fine spatial resolution can be provided by satellite synthetic aperture radar (SAR) operating at a frequency of 5.3 GHz (wavelength 5.6 cm), i.e. in C-band (Onstott and Shuchmann, 2004; Rees, 2006; Johannessen and others, 2007). Ice types and radar backscatter values obtained with C-band SAR or satellite scatterometer were correlated in various studies for the Arctic and Antarctic (Carsey and others, 1992; Kwok and others, 1992; Jeffries and others, 1995; Drinkwater and Lytle, 1997; Tsatsoulis and Kwok, 1998; Drinkwater and Liu, 2000; Kwok and others, 2003). During (cold) winter conditions ice-type discrimination is relatively straightforward because the typically shallow and dry snow cover has only a small influence on the radar backscatter at C-band. However, during summer or summer-like conditions this discrimination is hampered by an increasing influence of the snow cover.

Haas (2001) investigated C-band scatterometer data obtained over perennial sea-ice regions around Antarctica and found a marked increase in C-band radar backscatter values by, on average, 5.6 dB between spring (–16.3 dB) and summer (–10.7 dB); sudden drops in C-band radar backscatter values during spring/summer were also observed. According to Haas (2001), the increase is most likely caused by snow meltwater. A layer of superimposed ice is formed from refreezing snow meltwater percolating through the snow layer. This ice layer contains air bubbles and is rough at the centimeter scale. The above-mentioned sudden drops, on the other hand, can be associated with periods of a meltwater-saturated surface snow layer. These observations are confirmed by Kawamura and others (2006) who investigated C-band SAR data in relation to the snow property changes on landfast sea ice in Lützow-Holm Bay, Antarctica, and who reported minimum C-band normalized radar cross-section (NRCS) values during mid-summer and a remarkable increase in the NRCS values at the end of summer.

Willmes and others (2006, 2009) investigated snow properties on second-year ice in the Weddell Sea during mid-summer. They confirmed the initial decrease in C-band NRCS values once snowmelt commences and observed an increase in the NRCS values as summer progresses. This increase was caused by an increase in snow-grain size due to snow metamorphism triggered by diurnal melt–refreeze cycles. In addition to an increase in C-band NRCS values, brightness temperatures (TB) measured by the Special Sensor Microwave/Imager (SSM/I) at a frequency of 37 GHz, vertical polarization, start to vary diurnally once melt–refreeze cycles have set in. Willmes and others (2009) used this diurnal variation, together with the fact that an increased snow wetness also causes a substantial increase in TB(37 GHz) values (see Garrity, 1992), to characterize the nature and map the progress of snowmelt on Antarctic sea ice.

On Antarctic sea ice, surface flooding and formation of a slush layer on top of the sea ice under the submergence of
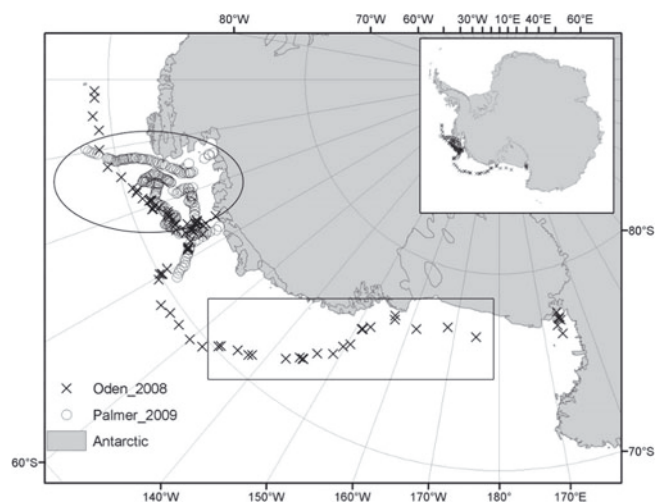
Fig. 1. Cruise tracks of *Oden* 2008 (total of 100 ship-based observations) and *Palmer* 2009 (total of 197 ship-based observations). The superposed ellipse and rectangle denote the approximate sample locations discussed in the paper.

sea ice due to a heavy snow load (Eicken and others, 1994) is quite common. The effect of ice–snow interface flooding with sea water on the radar backscatter of sea ice is, however, not yet fully understood. It is a function of various factors like frequency and incidence angle as well as processes at the ice–snow interface like brine wicking or slush-ice formation (Jeffries and others, 1995; Lytle and others, 1996; Morris and others, 1998; Haas, 2001; Onstott and Shuchmann, 2004).

With a –5.7% declining trend in sea-ice cover during 1979–2006, the Bellingshausen/Amundsen Seas region has shown the largest decline in Antarctic sea-ice extent (Comiso and Nishio, 2008). This contrasts with sea-ice extent increase rates of 4.2% in the Ross Sea region and 1.0% for the Southern Hemisphere overall (Comiso and Nishio, 2008). The objectives of this study are (1) to derive relationships between visual ship-based Antarctic Sea Ice Processes and Climate (ASPeCt) observations and coincident C-band NRCS values for different sea-ice types under mid- to late-summer conditions; (2) to explain the change in C-band NRCS values as summer progresses, with the aid of ASPeCt observations and Advanced Microwave Scanning Radiometer–Earth Observing System (AMSR-E) TB(37 GHz) values for the transition period from early summer to the end of summer in West Antarctic sea ice; and (3) to investigate the ridged-ice fraction and volume effect on C-band NRCS values. To address these objectives we use data collected on two research cruises, *Oden* 2008 and *Palmer* 2009, conducted in the West Antarctic sea-ice zone (Fig. 1) during the International Polar Year (IPY). In addition, we use European Space Agency (ESA) Environmental Satellite (Envisat) Advanced Synthetic Aperture Radar (ASAR) Wide Swath Mode (WSM) images and daily TB and sea-ice concentration values from the AMSR-E.

DATA

ASPeCt ship-based observations during *Oden* 2008 and *Palmer* 2009

Visual ship-based sea-ice observations constitute the main ground-truth data of this study. These were performed based on the ASPeCt protocol (Worby and others, 1999). ASPeCt

provides a consistent and quantifiable method for estimating the type, thickness and distribution of sea ice along a ship's track through the pack ice by making hourly observations from the ship's bridge. These observations include the ship's position, total sea-ice concentration, an estimate of the areal coverage, type, thickness, floe size, topography of sea ice and snow cover and depth in the three dominant ice-thickness categories within a ~1 km radius of the ship (Worby and others, 1999; Worby and Ackley, 2000). They are recorded on log sheets based on the predefined ASPeCt codes.

ASPeCt observations of *Oden* 2008 started on 10 December 2008 at 1200 h GMT and ended on 9 January 2009 at 0250 h GMT (austral summer). A total of 100 ASPeCt observations were carried out, as shown (by an x) in Figure 1. Total ice concentration and the primary (i.e. largest) ice-thickness ASPeCt observations during the cruises are presented in Figure 2a and b. During *Oden* 2008, average air temperature was $-2.5 \pm 1.8°C$; the minimum and maximum air temperatures were $-6.2°C$ and $3.9°C$. Average wind speed was $4.4 \pm 3.2 \, m \, s^{-1}$, with a maximum of $18 \, m \, s^{-1}$. Figure 3a shows the air-temperature values obtained from ASPeCt observations of *Oden* 2008.

A total of 197 ASPeCt observations were carried out during *Palmer* 2009, starting on 11 January 2009 at 1700 h GMT and ending on 16 February 2009 at 0000 h GMT. This period coincides with the second half of the 2009 austral summer; air temperatures varied between $-7.3°C$ and $1.9°C$, with a mean value of $-2.5 \pm 1.9°C$ (Fig. 3b). Average wind speed was $6.9 \pm 2.6 \, m \, s^{-1}$, with a maximum value of $10 \, m \, s^{-1}$. ASPeCt observations of total ice concentrations and the primary ice thicknesses are presented in Figure 4a and b, respectively. During *Oden* 2008 and *Palmer* 2009, in ~90% of all ASPeCt observations the primary ice type coincided with the dominant ice type.

Envisat ASAR WSM and AMSR-E brightness temperature

The ASAR instrument aboard the polar-orbiting Envisat satellite operates at C-band (frequency 5.3 GHz, wavelength 5.6 cm) (http://envisat.esa.int/instruments/asar/). Among its different operational modes, the WSM, having a nominal pixel spacing of 75 m with a spatial resolution of 150 m and a swath width of ~400 km, is the most appropriate for sea-ice monitoring (Johannessen and others, 2007). Here we use 15 ASAR WSM images obtained from ESA.

The AMSR-E aboard the polar-orbiting Aqua satellite is a microwave radiometer. The US National Snow and Ice Data Center (NSIDC) provides gridded AMSR-E/Aqua daily TB values, sea-ice concentration and snow depth data (AE_SI12) with a grid resolution of 12.5 km × 12.5 km. AE_SI12 includes horizontally and vertically polarized TB from 18.7 GHz through 89.0 GHz (D.J. Cavalieri and others, http://nsidc.org/data/ae_si12.html). From the AE_SI12 dataset, we used the ascending, descending and daily average TB(37 GHz) vertical polarization (TB37V henceforth), and the sea-ice concentration values.

METHODOLOGY

Worby and others (1998) indicated that daily shifts in ice-edge location may reach up to 1° of latitude in Antarctica. Thus, to reduce the inaccuracies that may arise from sea-ice advection between an ASPeCt observation and ASAR image acquisition, only those ASPeCt observations lying within
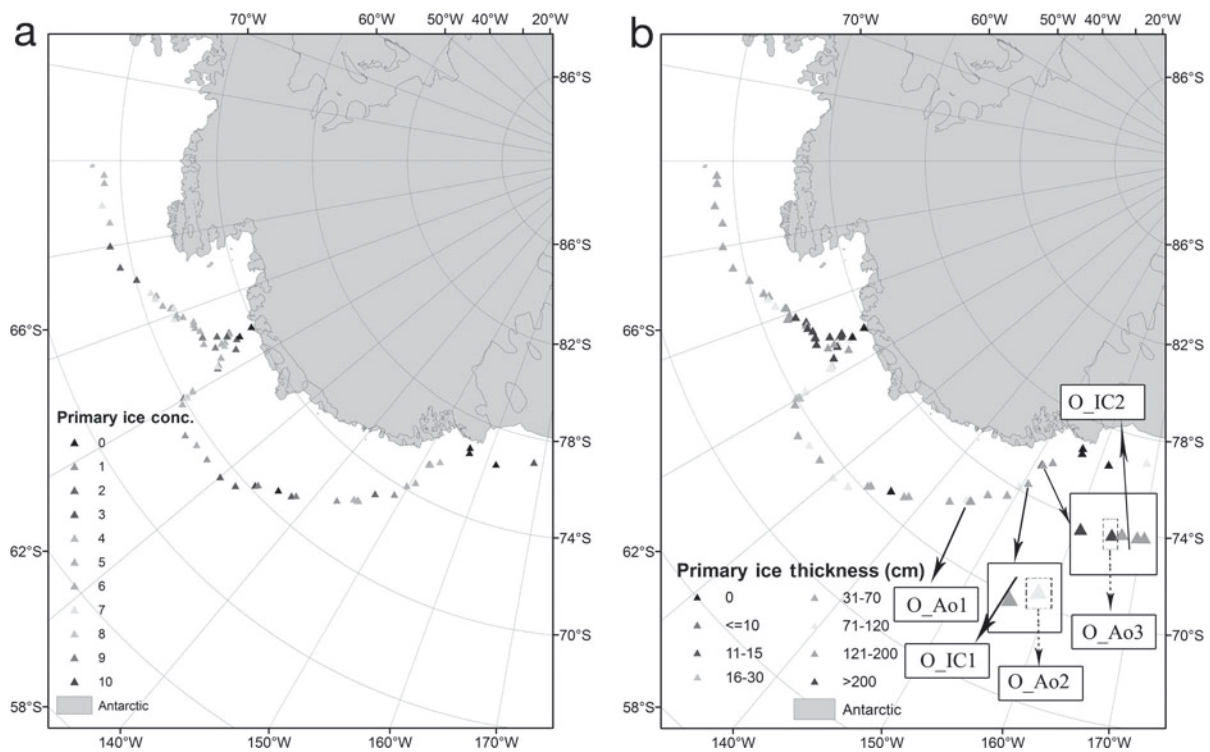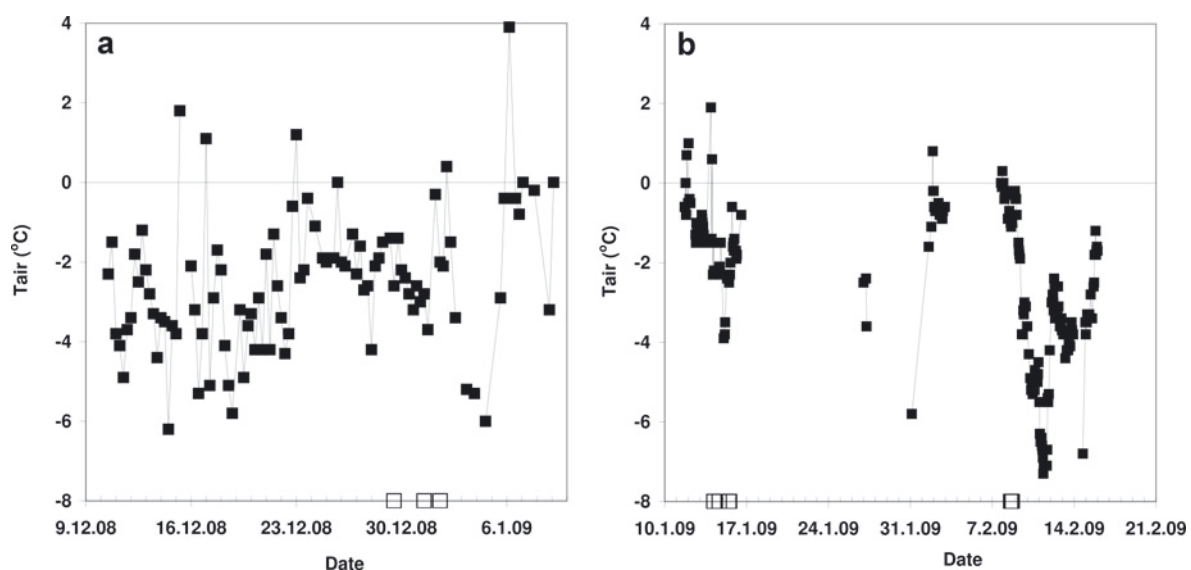
Fig. 2. Primary ice-concentration (a) and primary ice-thickness (b) from ASPeCt ship-based observations during *Oden* 2008. Sampling locations (ASPeCt as well as ice-core sampling) are denoted by arrows and boxes in (b). Each box in (b) is annotated with a code name that corresponds to entries in Table 1 and 2; 'IC' refers to an ice core, 'Ao' to an ASPeCt observation.

±2.5 hours of the ASAR image acquisition time are considered, resulting in eight images for comparison (Table 1). These images were geocoded, calibrated and projected onto a polar stereographic grid true at 70° S with a grid resolution of 125 m × 125 m.

Kwok and others (1992) noted the effect of wind-induced surface roughness on radar backscatter measurements over open water leading to ambiguities in interpretation of SAR images. Furthermore, icebreakers try to avoid the thickest ice during cruises, resulting in a bias towards thinner ice (Perovich and others, 2009). Thus, to reduce the ambiguities

arising from surface scattering over open water, only those ASPeCt data that have at least 50% total ice concentration are considered in the further analyses.

A 2.125 km × 2.125 km box (2 km × 2 km henceforth) centered at the ship's position for the corresponding ASPeCt observation was co-located in the respective ASAR image and is used to derive a mean C-band NRCS value for the respective 1 km ASPeCt observation radius. A typical histogram of such a box is given in Figure 5a. The standard deviation of the radar backscatter within the boxes is also calculated. However, within these 2 km × 2 km boxes comprising

Fig. 3. Air-temperature values for *Oden* 2008 (a) and *Palmer* 2009 (b) cruises. Dates are day.month.year. Open squares on the *x*-axis indicate the ASAR image acquisition.
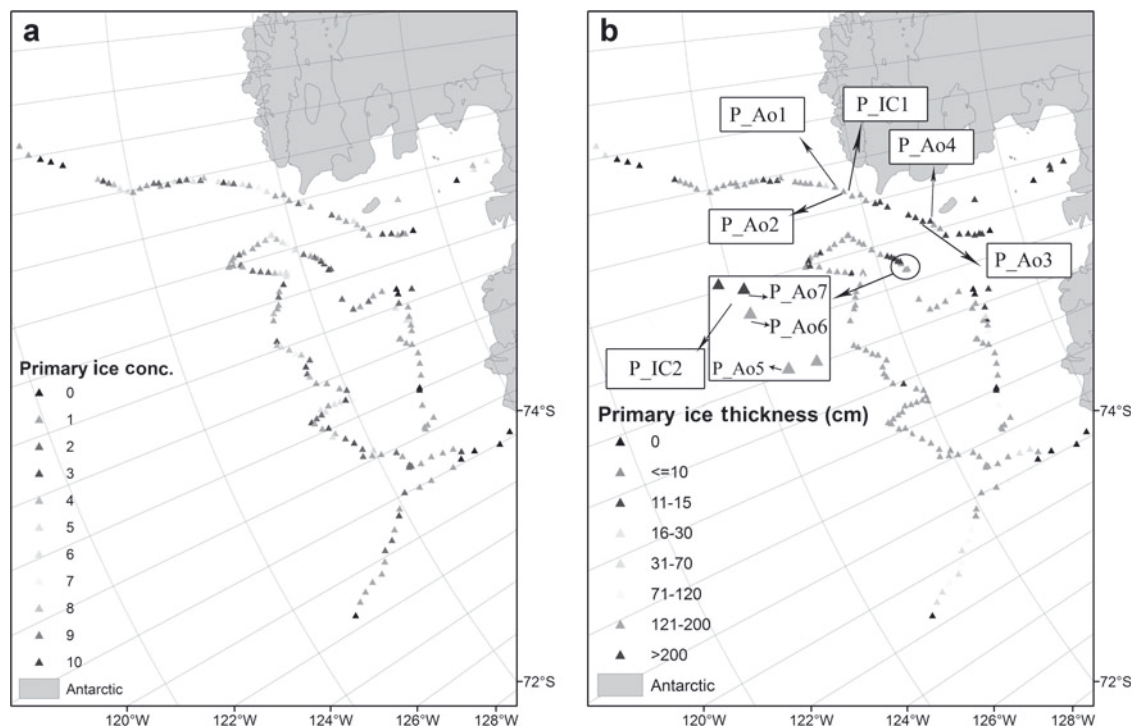
Fig. 4. Primary ice-concentration (a) and primary ice-thickness (b) ASPeCt ship-based observations during *Palmer* 2009. See Figure 2 caption for explanation of the boxes and code names.

289 SAR gridcells with 125 m grid resolution) more than one ice type or open water may exist. Consequently, a histogram of the NRCS distribution of such a 2 km × 2 km box might show more than one mode, so the mean NRCS value might be based on a mixture of different surface types, each with a distinct typical NRCS value (Fig. 5b). When the time difference between ASAR image acquisition and ASPeCt observations was >0.5 hour, and when neither the histogram

nor the 2 km × 2 km NRCS boxes provided a clear NRCS partitioning for different surface types, we looked into the NRCS distribution within 12.5 km × 12.5 km boxes centered at the ship's position and the respective histograms. In this way, features such as floe boundaries or the location of the ship could be better identified and the representativeness of the NRCS value for the ice conditions within the particular 2 km × 2 km box could be judged.

Table 1. Overview of observed (ASPeCt) total and dominant-ice-type ice concentrations (ice types are first-year ice (FY; thickness 0.7–1.2 m), thick first-year ice (TFY; thickness >1.2 m) and multi-year ice (MY)) and dominant-ice-type thickness and snow depth, together with mean values and standard deviations of ASAR radar backscatter (NRCS) for the available overlapping dates. The ASAR incidence angle, α, is the local incidence angle (degrees from nadir) at the ship's position. The number of pixels is the number of valid ASAR image gridcells of the respective 2 km × 2 km box (maximum number here is 288; a smaller number indicates that the box is located at the ASAR image edge)

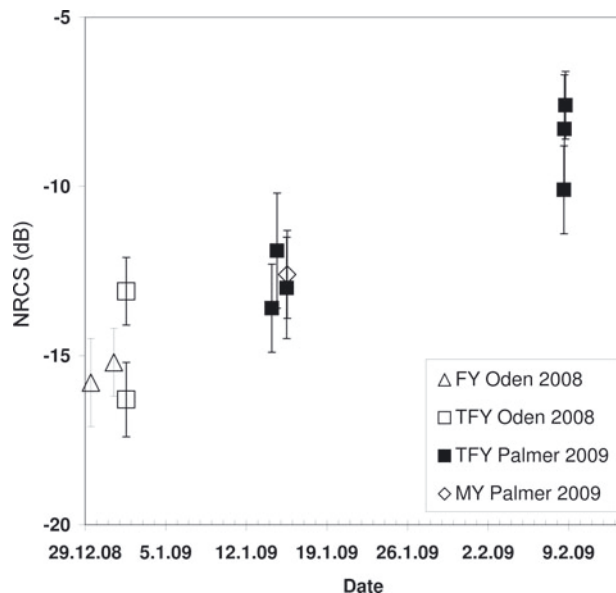| Cruise	Date	ASPeCt observations						ASAR data				Code in Figs 2 and 4
		Time (UTC)	Total conc.	Dominant ice type				Time (UTC)	NRCS		N	α	
				Conc.	Type	Thickness			mean	s.d.			
						Ice	Snow						
		h	1/10	1/10		m	m	h	dB	dB		°	
Oden 2008	29 Dec 2008	1200	5	5	FY	1.0	0.5	1112	−15.8	1.3	191	41	O_Ao1
	31 Dec 2008	1200	6	6	FY	1.0	0.4	1149	−15.2	1.0	225	34	O_Ao2
	1 Jan 2009	1330	6	6	TFY	2.5	0.4	1118	−13.1	1.0	281	23	O_Ao3
		1330	6	6	TFY	2.5	0.4	1257	−16.3	1.1	238	40	
Palmer 2009	14 Jan 2009	500	7	7	TFY	2.0	0.2	749	−13.6	1.3	135	32	P_Ao1
		1600	5	5	TFY	2.0	0.7	1424	−11.9	1.7	288	21	P_Ao2
	15 Jan 2009	1200	5	2	TFY	1.5	0.4	1352	−13.0	1.5	236	31	P_Ao3
		1300	7	5	MY	4.0	1.5		−12.6	1.3	183		P_Ao4
		1400	5	3	TFY	1.5	0.5		−10.1	1.3	288		P_Ao5
	8 Feb 2009	1500	7	3	TFY	2.0	0.7	1438	−8.3	1.6	277	21	P_Ao6
		1700	8	5	TFY	2.5	0.7		−7.6	1.0	283		P_Ao7
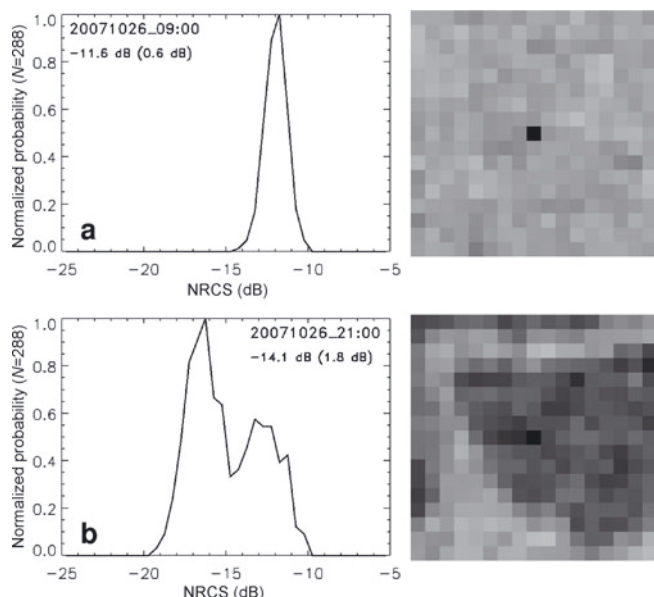
Fig. 5. Histograms of the C-band HH-polarization radar backscatter (left) distribution shown in the maps (right) for a unimodal case (a) and a bimodal case (b). Note that while the mean value is quite close to the modal value in (a) it is not in (b) but would represent an ice-type mixture with NRCS of about –16 dB and –13 dB.

Fig. 6. Time series of C-band HH-polarization radar backscatter (NRCS) with ±1 standard deviation observed during *Oden* 2008 and *Palmer* 2009 for multi-year ice (diamonds) and thick first-year ice (squares). Dates are day.month.year.

OBSERVED NRCS VALUES

The dominant ice types, concentrations, the mean and standard deviations (± s.d.) of the NRCS values obtained are listed in Table 1. Figure 6 represents the time series of NRCS values (mean ± s.d.) for the encountered ice types: multi-year (MY), first-year (FY) and thick first-year (TFY) ice. NRCS values obtained from 2 km × 2 km boxes for TFY range from –16.3 ± 1.1 to –7.6 ± 1.0 dB; the maximum standard deviation for TFY is 1.7 dB. Just one NRCS value was obtained for MY ice: –12.6 ± 1.3 dB. Note that the NRCS values of TFY increase with time from ∼–15 dB in December/January to –9 dB in mid-February.

In addition to the ASAR images co-located with ASPeCt observations, we have four ice cores with an ASAR overpass within 2 hours. Respective parameters are listed in Table 2. The ice type for ice cores is either FY or TFY ice. Snow depths and conditions at the snow–ice interface were,

however, quite variable and we have to distinguish between flooded and non-flooded cases. During the *Oden* 2008 cruise, the NRCS takes values of –16.3 dB over TFY ice with just 3 cm of snow, and –14.9 dB over TFY ice with 52 cm of snow, both without flooding but with slush present at the snow–ice interface (December/January). During the *Palmer* 2009 cruise, the NRCS takes values between –13.6 and –8.0 dB over flooded FY or TFY ice with a deep snowpack (41 and 76 cm). Note that the lower value has been observed in mid-January, while the higher value (–8.0 dB) has been observed towards mid-February. Therefore, as shown in Figure 6, an increase of the NRCS over time can be observed. Note that, for both Figure 6 and Table 2, ASAR images were acquired at air temperatures below 0°C. However, for the second (1 January; code O_IC2), third (14 January; code P_IC1) and last (8 February; code P_IC2) cores given in Table 2, air temperatures were close to or at the freezing point a few hours prior to core sampling and ASAR image acquisition (see Fig. 3a and b). For the second

Table 2. Comparison of ice-core ice and snow properties and the co-located ASAR C-band HH-polarization radar backscatter value (NRCS) for *Oden* 2008 and *Palmer* 2009. ASPeCt ice types FY and TFY denote first-year ice (thickness 0.7–1.2 m) and thick first-year ice (thickness >1.2 m), respectively

Cruise	Date	ASPeCt and in-situ observations					ASAR		Tair	Code in Figs 2 and 4
		Time (UTC)	Type	Thickness		Freeboard	Note	Time (UTC)	NRCS		
				Ice	Snow						
		h		m	m	m		h	dB	°C	
Oden 2008	31 Dec 2008	1233	TFY	1.77	0.52	–	[a]	1149	–14.9	–3.1	O_IC1
	1 Jan 2009	1431	TFY	1.44	0.03	–	[b]	1257	–16.3	–1.9	O_IC2
Palmer 2009	14 Jan 2009	645	FY	0.88	0.41	–0.08	flooded	749	–13.6	–2.2	P_IC1
	8 Feb 2009	1635	TFY	1.35	0.76	–0.26	flooded	1438	–8.0	–1.0	P_IC2

[a] 5 cm slush at snow–ice interface; top 28 cm of ice core is also slushy.
[b] No slush at top; instead the top 18 cm of the ice core are porous, slushy intervals from 60 to 100 cm and at the bottom.
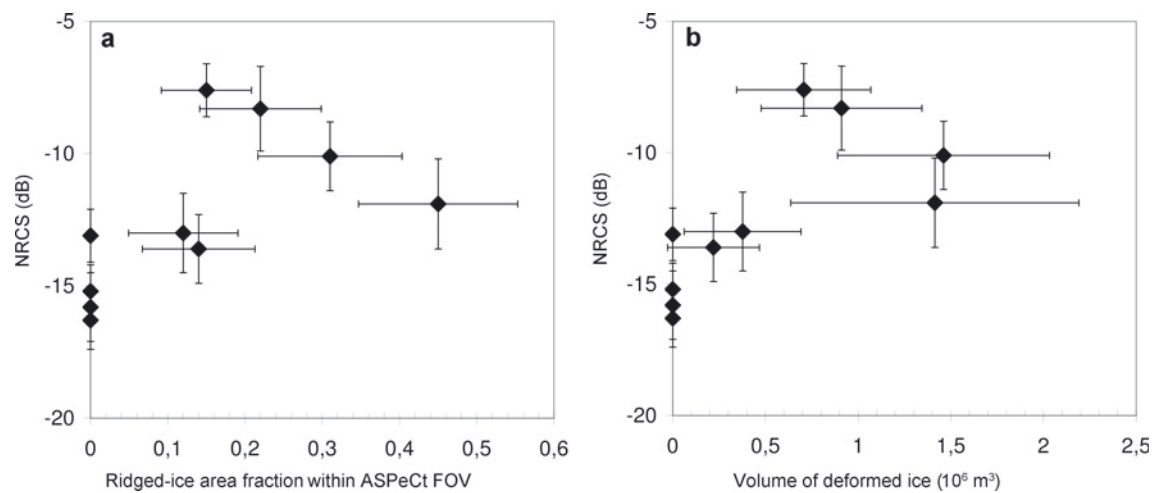
Fig. 7. Variation of C-band HH-polarization radar backscatter with ridged-ice area (a) and with volume of deformed ice (b) within ASPeCt's 1 km observation radius (field of view (FOV)) around the ship. Error bars denote one standard deviation.

and fourth cores (O_IC2, P_IC2; Table 2) the ASAR image acquisition was before the core sampling, i.e. closer to the observed higher air temperatures.

INTERPRETATION AND DISCUSSION

The observed range of C-band NRCS values for FY and TFY ice (Table 2) agrees with other summertime sea-ice NRCS observations in the West Antarctic (e.g. Morris and others, 1998). This range includes the NRCS value of −12.4 ± 0.6 dB found by Ozsoy-Cicek and others (in press) for late-winter/early-spring conditions in the Bellingshausen Sea. The observed increase in C-band radar backscatter values with time (Fig. 6) agrees with the findings of Haas (2001) and Kawamura and others (2006). The radar backscatter value observed for MY ice (Table 2), −12.6 ± 1.3 dB, is also in agreement with earlier summertime observations of C-band radar backscatter (Morris and others, 1998; Haas, 2001). Note that this value has higher standard deviation than that given by Ozsoy-Cicek and others (in press) for late-winter/early-spring conditions.

A substantial fraction of the large difference (3.2 dB) between the NRCS values for region O_Ao3 (Table 1; Fig. 2b) is likely caused by the incidence angle difference: 23° versus 40° (Table 1). According to Nghiem and Bertoia (2001) and Stern and Moritz (2002), typical changes of C-band HH-polarization radar backscatter over Arctic FY and MY ice are ∼1.5 and ∼1.0 dB per 10° incidence angle, respectively. Assuming that a similar change rate is applicable for Antarctic sea ice, this would result in a decrease in the NRCS of the order of 2 dB in the aforementioned case between the observations at 23° incidence angle and 40° incidence angle. NRCS values for O_Ao3 corrected for the incidence-angle influence would then read −15.1 ± 1.0 and −16.3 ± 1.1 dB; accordingly the values would almost agree within one standard deviation. Therefore the difference in incidence angles must be kept in mind when comparing NRCS values of the same ice type from different samplings. The differences between the NRCS values observed on 8 February (Table 1) could more likely be an artifact caused by the increasing time difference between ASPeCt observation and ASAR image acquisition; for the last value (−7.6 dB) this difference is >2 hours.

Figure 6 reveals that on 14/15 January during *Palmer* 2009, TFY and MY ice cannot be discriminated by means of the obtained C-band HH-polarization NRCS values. The spread between the values will reduce if we take the incidence-angle influence into account (MY ice: 31°; TFY ice: 21°, 31° and 32° (Table 1)). Despite the data being from different seasons, this result is similar to the findings of Ozsoy-Cicek and others (in press).

In the following, we discuss the observed range and temporal variation of the NRCS values in the context of the possible causes.

NRCS values versus ridged-ice fraction and volume

The sea-ice roughness is one of the factors that can influence C-band radar backscatter values. We calculated the areal fraction and the volume of ridged ice within the ASPeCt observation radius from the ASPeCt observations of the topography (*x* and *y* values of topography information in ASPeCt codes). For the areal fraction, this is done by considering the respective fraction of ridges within each of the three ice types observed, and calculating a weighted sum of the fraction of ridged ice. For the volume, the average sail height is also taken into account. Note that the volume only comprises the volume fraction above the level sea ice. Figure 7 displays the areal fraction (Fig. 7a) and the volume (Fig. 7b) for ASPeCt observations given in Table 1 together with the coincident C-band HH-polarization NRCS values. Larger fractions of ridged ice are associated with high C-band HH-polarization NRCS values according to observations carried out by Drinkwater and others (1995) and Jeffries and others (1995); both teams noted an increase in C-band radar backscatter values by ∼10 dB between undeformed and deformed FY ice. However, the spread in the values is large, as is the standard deviation of both the NRCS and the ridged-ice fraction. A similar picture is seen when looking at the volume (Fig. 7b): large volumes tend to be associated with higher C-band HH-polarization NRCS values.

NRCS values versus TB37V

High daily average TB37V values are typical for melting conditions, because the high liquid water content in the snow cover causes a high emissivity and thus high brightness temperatures; it also masks the emission from the underlying
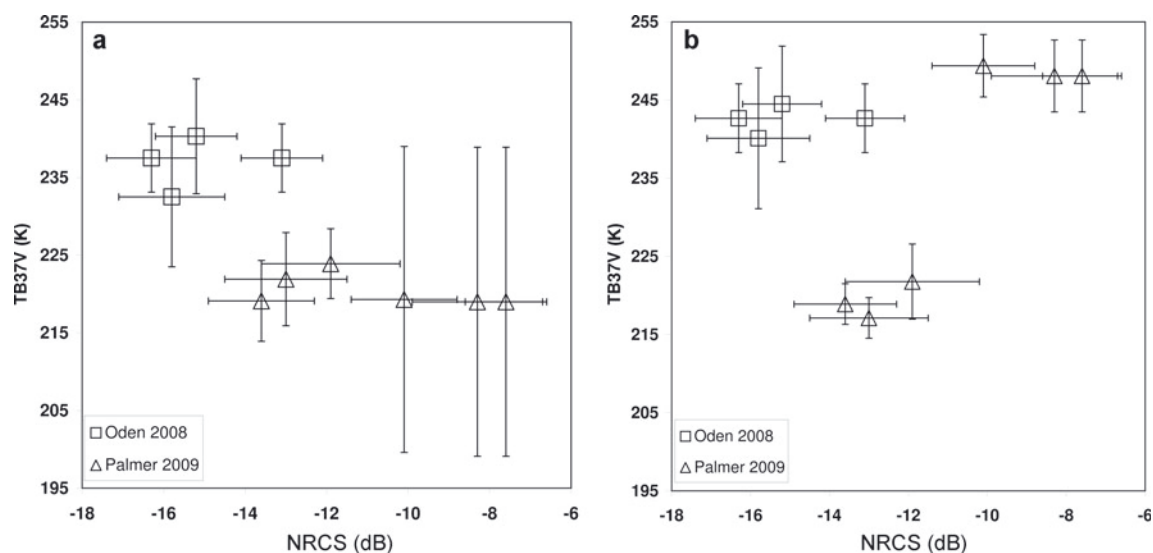
Fig. 8. AMSR-E TB37V values in comparison to co-located coincident ASAR C-band HH-polarization radar backscatter (NRCS) values using (a) a 7 day mean TB37V at the ship's position centered at the day of observation, and (b) a 1 day mean TB37V over a 3 × 3 gridcell area centered at the ship's position at the day of observation. Error bars denote one standard deviation (NRCS: variation within the 2 km box around the ship's position; TB37V: variation within the 7 day period (a) and variation within the 3 × 3 gridcell area (b)).

sea ice. In contrast, comparably low daily average TB37V values associated with an elevated diurnal variation of TB37V values indicate that melt–refreeze cycles have commenced (Willmes and others, 2006, 2009). These cycles cause alternating high (melting during the day) and low (refreezing during the night) liquid water contents in the snow; the low contents are additionally associated with coarse-grained snow which is known for a low emissivity and thus a lower brightness temperature than in the afore-mentioned case. Therefore we compare our observed C-band HH-polarization NRCS values with co-located AMSR-E TB37V values. To reduce the potential influence of a changing ice concentration on the co-located TB37V values, we used only those data pairs (TB37V, NRCS) where ice concentrations observed during ascending and descending AMSR-E overpasses varied by <25%.

Figure 8a displays 7 day average TB37V values taken from the nearest co-located 12.5 km gridcell, with the 7 day period centered at the day of ASPeCt observation and ASAR image acquisition. A 7 day average was used to reduce day-to-day TB variations due to changing weather conditions; this way the average situation is displayed. For *Oden* 2008, TB37V takes values around 237 K, while for *Palmer* 2009 on 14/15 January and 8 February, TB37V takes values of about 221 and 219 K, respectively. This decrease in TB37V makes sense, because *Oden* 2008 data were acquired in December/January, i.e. during peak melt season, while *Palmer* 2009 data were obtained later. Consequently, the liquid water content in the snow can be expected to be higher during *Oden* 2008 than during *Palmer* 2009, and thus higher TV37V values can be expected during *Oden* 2008 than during *Palmer* 2009. Note the extremely high standard deviation for TB37V values for *Palmer* 2009 on 8 February.

Figure 8b displays 1 day average TB37V values taken from a 3 × 3 gridcell box centered at the ship's position. For *Oden* 2008 and *Palmer* 2009, on 14/15 January, TB37V takes values similar to those shown in Figure 8a: 242 and 219 K. However, for *Palmer* 2009 on 8 February, TB37V

values are as high as 248 K, i.e. 30 K higher than the 7 day average value.

Table 3 summarizes the results of a similar comparison between NRCS values associated with the ice-core analysis (see Table 2) and co-located AMSR-E TB37V values. For each ice-core location, Table 3 gives for a 3 × 3 gridcell box centered at the ice-core location the daily average TB37V (column Tb), its standard deviation (=spatial variability; column s.d. Tb), the daily average ice concentration (column Ice con), and the difference between average TB37V values of the ascending and the descending over-passes (column Delta Tb) for an 8 day period ending 1 day after ice-core sampling.

For core 31 December 2008 and core 1 January 2009, high TB37V values are observed, similar to Figure 8a and b. The total TB37V range is small: 8.7 and 4.8 K, respectively. Standard deviations are relatively high, ~6 K, and are partly determined by the day-to-day variation in the mean ice concentration (squared linear correlation coefficient 0.41). TB37V differences between ascending and descending AMSR-E overpasses remain on average <4 K and are less associated with ice concentration variations (squared linear correlation coefficient 0.24); a decrease (increase) in ice concentration would cause a decrease (increase) in TB37V. Taking Figure 6 into account and the information about snow depth and ice–snow interface properties given in Table 2, we suggest that melt conditions prevailed during *Oden* 2008 since TB37V values were high and TB37V differences between ascending and descending overpasses were low.

For core 14 January 2009, TB37V values are similar to Figure 8a and b, being ~220 K, and indicate a range of 11.1 K, between 216.2 and 227.3 K. Standard deviations are ~4 K, smaller than for the other two ice cores with a lower and similarly variable ice concentration. However, TB37V differences are substantially larger, taking values between 8 and 18 K (average 11.2 ± 3.2 K). In comparison to the latter two cores (see above) we suggest that melt–refreeze has already commenced because TB37V values have dropped

Table 3. Daily mean and standard deviation of brightness temperatures (Tb and s.d. Tb, respectively), daily mean ice concentrations (Ice con) and daily brightness temperature amplitude (Delta Tb) obtained from AMSR-E; temperatures are given in K, ice concentrations in %

	Oden 2008 ice core 31 December 2008					Oden 2008 ice core 1 January 2009			
	Tb	Ice con	Delta Tb	s.d. Tb		Tb	Ice con	Delta Tb	s.d. Tb
25 Dec 2008	251.7	96.7	3.8	4.5	26 Dec 2008	245.1	91.1	3.4	5.7
26 Dec 2008	250.0	97.0	3.3	4.9	27 Dec 2008	243.2	88.6	2.1	6.3
27 Dec 2008	248.2	91.3	3.8	5.5	28 Dec 2008	242.6	89.9	3.0	6.3
28 Dec 2008	245.6	90.7	3.2	7.4	29 Dec 2008	242.9	91.2	1.8	5.5
29 Dec 2008	243.7	87.7	2.3	6.7	30 Dec 2008	242.1	91.4	3.8	5.3
30 Dec 2008	243.0	87.1	3.2	5.1	31 Dec 2008	242.1	95.3	3.9	5.3
31 Dec 2008	244.7	92.6	3.7	4.2	1 Jan 2009	240.3	97.0	3.0	5.1
1 Jan 2009	245.2	98.7	3.4	2.4	2 Jan 2009	241.4	96.1	4.7	5.6

	Palmer 2009 ice core 14 January 2009					Palmer 2009 ice core 8 February 2009			
	Tb	Ice con	Delta Tb	s.d. Tb		Tb	Ice con	Delta Tb	s.d. Tb
8 Jan 2009	220.8	86.9	8.8	2.9	2 Feb 2009	240.8	88.7	16.8	4.2
9 Jan 2009	217.8	82.9	9.5	3.1	3 Feb 2009	229.1	91.4	14.1	3.0
10 Jan 2009	220.5	79.0	10.8	5.8	4 Feb 2009	207.4	94.8	1.8	2.3
11 Jan 2009	219.5	89.0	9.6	3.7	5 Feb 2009	205.2	94.6	2.3	2.1
12 Jan 2009	227.3	85.4	18.0	2.0	6 Feb 2009	221.8	91.4	15.3	3.0
13 Jan 2009	225.9	88.3	12.6	2.5	7 Feb 2009	248.0	87.2	3.9	8.2
14 Jan 2009	217.9	75.0	12.6	4.9	8 Feb 2009	247.3	93.8	1.5	5.7
15 Jan 2009	216.2	84.0	8.0	4.6	9 Feb 2009	209.8	93.2	17.6	1.7

while TB37V differences have increased to values above 10 K, which is the value suggested by Willmes and others (2009) to indicate melt–freeze cycles.

Core 8 February 2009 reveals the most variable conditions: TB37V values vary from 205.2 to 248.0 K (i.e. over a range of 42.8 K), standard deviations take values between 1.7 and 8.2 K, and TB37V differences take values between 1.5 and 17.6 K (average 9.2 ± 7.4 K). This agrees very well with the discrepancy between the 7 day and 1 day average TB37V values shown for this date in Figure 8a and b. The average TB37V difference does not exceed the above-mentioned threshold of 10 K. However daily TB37V values switch between very low values (~2 K) and values that exceed the threshold considerably (at least 14 K). Therefore we suggest that melt–refreeze has further advanced and is still in progress (see also the low 7 day average TB37V values given in Fig. 8a) but that unlike for core 14 January 2009 it is disturbed. One possibility could be snow-property changes due to advection of warm air.

Note that the air temperatures shown in Figure 3a for *Oden* 2008 and in Figure 3b for *Palmer* 2009 are not really suitable to aid this interpretation because (1) the liquid water content in the snow is not just determined by the air temperature but also by internal snowmelt due to shortwave radiation, and (2) the given temperatures display the situation at the ship's location, which can vary substantially on a daily basis, and therefore the shown air-temperature time series cannot be used to explain surface conditions at a certain location 2 days before or after, for example, the ASAR image acquisition. We also note that air temperatures remained above –5°C all the time, so liquid water could have been present in the snow all the time (Garrity, 1992). To better interpret the remote-sensing data, more and detailed investigations of the snow properties during both cruises would have been very helpful.

CONCLUSIONS

We compared Envisat ASAR C-band HH-polarization radar backscatter (NRCS) values with results from ice-core analysis and visual ship-based observations of sea-ice and snow properties carried out according to the ASPeCt protocol in the Bellingshausen and Amundsen Seas during two cruises (*Oden* 2008, *Palmer* 2009) in austral summer 2008/09. The dominant ice types encountered were TFY and MY ice, both with a snow cover typically several tenths of a meter thick. Flooding of the ice–snow interface was observed occasionally. The NRCS values obtained for MY (TFY) ice are 12.6 ± 1.3 dB (-16.3 ± 1.1 dB to -7.6 ± 1.0 dB) and thus fall within the ranges reported in earlier studies dealing with summer Antarctic sea ice (e.g. Morris and others, 1998). Average radar backscatter values for TFY increase from ~–15 dB in December/January to ~–9 dB in February, in agreement with findings by Haas (2001) for perennial ice in the Bellingshausen Sea and results by Kawamura and others (2006) for fast ice in Lützow-Holm Bay.

The in situ observations of the snow and ice properties carried out during both cruises (ice cores and ASPeCt observations) as well as the observed meteorological parameters (e.g. air temperature) are not sufficient alone to interpret the observed radar backscatter values and their variation over time. We compared the radar backscatter values with the fraction of ridged ice and the associated ice volume derived from the ASPeCt observations. We found an indication that C-band HH-polarization radar backscatter values increase with increasing fraction of ridged ice (and volume). However, the investigated dataset is far too small to draw a conclusion; the scatter in the observed values as well as the NRCS values is too large.

We observed an increase in the C-band HH-polarization radar backscatter over time, which is accompanied by a

drop in the 7 day average of co-located AMSR-E TB37V over time. This is consistent with the assumption that melt is at its peak in December/January, causing high liquid water content in the snow and thus high TB37V values/low C-band radar backscatter values. In February melt–refreeze cycles have commenced, causing a coarse-grained snow cover and thus a drop in TB37V values/high C-band radar backscatter values. This assumption is underlined by the fact that the difference in TB37V values between ascending and descending AMSR-E overpasses is ∼4 K in December/January. However, starting in mid-January, values exceed the 10 K threshold given by Willmes and others (2009) as the indicator for melt–refreeze cycles. Thus, although the in situ observations of the ice and snow properties are very sparse we are confident the temporal radar backscatter change was caused by the transition from melt conditions to the commencement of melt–refreeze cycles.

Although it seems likely that snow-wetness changes and snow metamorphism have played the dominant role for the observed changes in C-band HH-polarization radar back-scatter and in TB37V, more information about the vertical snow structure and its temporal evolution would be an asset for any interpretation of similar data in the future. It should be kept in mind that this study is just a case study, involving only 11 data pairs of in situ and satellite observations and as such its results must not be over-interpreted. If a similar study is planned for the future in the region encountered here, it should follow the examples given by the Ice Station POLarstern (ISPOL; Hellmer and others, 2008) and Sea Ice Mass Balance in the Antarctic (SIMBA; Lewis and others, in press) cruises, during which detailed snow property obser-vations were carried out on a drifting ice camp for a few weeks. However, instead of looking at just one ice floe we recommend trying to set up an array of automatic measurement stations (temperature profile in snow and ice, snow depth and ice thickness (by ice mass-balance buoy), short- and longwave radiation) at locations which (1) are spatially distributed over an area of several AMSR-E 12.5 km × 12.5 km gridcells, and (2) represent the dominant ice type of that particular region. At regular time intervals and on demand (e.g. when meteorological conditions change rapidly), these locations should be visited to obtain snow and ice samples to identify changes in the vertical layering (e.g. slush/ no-slush, flooding /no-flooding, density and grain-size changes) in the ice–snow system. A pre-requisite that should not be overlooked in this context is the proper planning of SAR data acquisition in order to have a reasonable temporal and regional coverage with SAR data as was realized during SIMBA.

ACKNOWLEDGEMENTS

REFERENCES

Carsey, F.D *and 7 others, eds.* 1992. *Microwave remote sensing of sea ice.* Washington, DC, American Geophysical Union.

Comiso, J.C. and F. Nishio. 2008. Trends in the sea ice cover using enhanced and compatible AMSR-E, SSM/I, and SMMR data. *J. Geophys. Res.,* **113**(C2), C02S07. (10.1029/2007JC004257.)

Drinkwater, M.R. and X. Liu. 2000. Seasonal to interannual variability in Antarctic sea-ice surface melt. *IEEE Trans. Geosci. Remote Sens.,* **38**(4), 1827–1842.

Drinkwater, M.R. and V.I. Lytle. 1997. ERS-1 radar and field-observed characteristics of autumn freeze-up in the Weddell Sea. *J. Geophys. Res.,* **102**(C6), 12,593–12,608.

Drinkwater, M.R., R. Hosseinmostafa and P. Gogineni. 1995. C-band backscatter measurements of winter sea-ice in the Weddell Sea, Antarctica. *Int. J. Remote Sens.,* **16**(17), 3365–3389.

Eicken, H., M.A. Lange, H.W. Hubberten and P. Wadhams. 1994. Characteristics and distribution patterns of snow and meteoric ice in the Weddell Sea and their contribution to the mass balance of sea ice. *Ann. Geophys.,* **12**(1), 80–93.

Garrity, K. 1992. Characterization of snow on floating ice and case studies of brightness temperature change during the onset of melt. In Carsey, F.D. *and 7 others, eds. Microwave remote sensing of sea ice.* Washington, DC, American Geophysical Union, 313–328.

Haas, C. 2001. The seasonal cycle of ERS scatterometer signatures over perennial Antarctic sea ice and associated surface ice properties and processes. *Ann. Glaciol.,* **33**, 69–73.

Hellmer, H.H., M. Schröder, C. Haas, G.S. Dieckmann and M. Spindler. 2008. The ISPOL drift experiment. *Deep-Sea Res. II,* **55**(8–9), 913–917.

Jeffries, M.O., *ed.* 1998. *Antarctic sea ice: physical processes, interactions and variability.* Washington, DC, American Geophysical Union. (Antarctic Research Series 74.)

Jeffries, M.O., T.S. Chuah and K. Morris. 1995. C-band radar backscatter from Antarctic first-year sea ice: 1. *In situ* scatterometer measurements. *Antarct. J. US,* **30**(1–4), 24–26.

Johannessen, O.M. *and 9 others.* 2007. *Remote sensing of sea ice in the Northern Sea route.* Chichester, Praxis Publishing.

Kawamura, T., H. Wakabayashi and S. Ushio. 2006. Growth, properties and relation to radar backscatter coefficient of sea ice in Lützow-Holm Bay, Antarctica. *Ann. Glaciol.,* **44**, 163–169.

Kwok, R., E. Rignot, B. Holt and R. Onstott. 1992. Identification of sea ice types in spaceborne synthetic aperture radar data. *J. Geophys. Res.,* **97**(C2), 2391–2402.

Kwok, R., G.F. Cunningham and S.V. Nghiem. 2003. A study of the onset melt over the Arctic Ocean in RADARSAT synthetic aperture data. *J. Geophys. Res.,* **108**(C11), 3363. (10.1029/2002JC001363.)

Lewis, M.J. *and 6 others.* In press. Sea ice and snow cover characteristics during the winter–spring transition in the Bellingshausen Sea: an overview of SIMBA 2007. *Deep-Sea Res. II.* (10.1016/j.dsr2.2010.10.027.)

Lubin, D. and R. Massom. 2006. *Polar remote sensing. Volume 1: atmosphere and oceans.* Chichester, Springer-Praxis.

Lytle, V.I., K.C. Jezek, S.P. Gogineni and A.R. Hosseinmostafa. 1996. Field observations of microwave backscatter from Weddell Sea ice. *Int. J. Remote Sens.,* **17**(1), 167–180.

Meier, W.N. and J. Stroeve. 2008. Comparison of sea-ice extent and ice-edge location estimates from passive microwave and en-hanced-resolution scatterometer data. *Ann. Glaciol.,* **48**, 65–70.

Morris, K., M.O. Jeffries and S. Li. 1998. Sea ice characteristics and seasonal variability of ERS-1 SAR backscatter in the Bellings-hausen Sea. In Jeffries, M.O., *ed. Antarctic sea ice: physical processes, interactions and variability.* Washington, DC, Ameri-can Geophysical Union, 213–242. (Antarctic Research Series 74.)

Nghiem, S.V. and C. Bertoia. 2001. Study of multipolarization C-band backscatter signatures for Arctic sea ice mapping with future satellite SAR. *Can. J. Remote Sens.,* **27**(5), 387–402.

Onstott, R.G. and R.A. Shuchmann. 2004. SAR measurements of sea ice. *In* Jackson, C.R. and J.R. Apel, *eds. Synthetic aperture radar marine user's manual.* Washington DC, US Department of Commerce. National Oceanic and Atmospheric Administration; National Environmental Satellite, Data, and Information Service, 81–116.

Ozsoy-Cicek, B., S. Kern, S.F. Ackley, H. Xie and A.E. Tekeli. In press. Intercomparisons of Antarctic sea ice types from visual ship, RADARSAT-1SAR, Envisat ASAR, QuikSCAT, and AMSR-E satellite observations in the Bellingshausen Sea. *Deep-Sea Res. II.* (10.1016/j.dsr2.2010.10.031.)

Perovich, D.K. *and 7 others.* 2009. Transpolar observations of the morphological properties of Arctic sea ice. *J. Geophys. Res.,* **114**, C00A04. (10.1029/2008JC004892.)

Rees, W.G. 2006. *Remote sensing of snow and ice.* Boca Raton, FL, CRC Press.

Smith, S.D., R.D. Muench and C.H. Pease. 1990. Polynyas and leads: an overview of physical processes and environment. *J. Geophys. Res.,* 95(C6), 9461–9479.

Stern, H.L. and R.E. Moritz. 2002. Sea ice kinematics and surface properties from RADARSAT synthetic aperture radar during the SHEBA drift. *J. Geophys. Res.,* **107**(C10), 8028. (10.1029/2000JC000472.)

Tsatsoulis, C. and R. Kwok. 1998. *Analysis of SAR data of the polar oceans: recent advances.* Berlin, etc., Springer-Verlag.

Willmes, S., J. Bareiss, C. Haas and M. Nicolaus. 2006. The importance of diurnal processes for the seasonal cycle of sea-ice microwave brightness temperatures during early summer in the Weddell Sea, Antarctica. *Ann. Glaciol.,* **44**, 297–302.

Willmes, S., C. Haas, M. Nicolaus and J. Bareiss. 2009. Satellite microwave observations of the interannual variability of snowmelt on sea ice in the Southern Ocean. *J. Geophys. Res.,* **114**(C3), C03006. (10.1029/2008JC004919.)

Worby, A.P. and S.F. Ackley. 2000. Antarctic research yields circumpolar sea ice thickness data set. *Eos,* **81**(17), 181,184–181,185.

Worby, A.P., R.A. Massom, I. Allison, V.I. Lytle and P. Heil. 1998. East Antarctic sea ice: a review of its structure, properties and drift. *In* Jeffries, M.O., *ed. Antarctic sea ice: physical processes, interactions and variability.* Washington, DC, American Geophysical Union, 41–67. (Antarctic Research Series 74.)

Worby, A.P., I. Allison and V. Dirita. 1999. A technique for making ship-based observations of Antarctic sea ice thickness and characteristics. Part I. Observational techniques and results. *Antarct. CRC Res. Rep.* 14.